scientific reports

OPEN

Spondias pinnata mediated silver nanoparticles with antibiofilm and catalytic potential

Bijoy Krishna Das[1,2], Manash Chandra Das[3], Sourav Ghosh[4,5], Rajesh Debnath[1], Antony Gomes[4] & Utpal Chandra De[1✉]

In the quest for advancing bio-conjugated metal nanoparticle synthesis as a promising avenue in biochemistry, this study emphasizes the optimized fabrication of silver nanoparticles mediated by *Spondias pinnata*. The synthesized silver nanoparticles (SP-AgNPs) exhibited remarkable colloidal stability for 6–7 months at ambient temperature (25 ± 4 °C) supported by a highly negative zeta potential of -37 mV. Characterization *via* HR-TEM, XRD, XPS, ICP-OES, and DLS studies confirmed the spherical morphology of the SP-AgNPs, with an average diameter of 32 ± 5 nm and a face-centered cubic (fcc) arrangement of particles. The SP-AgNPs demonstrated significant antibacterial and antibiofilm activity against *Escherichia coli* (*E. coli*) MTCC 118 strain and catalytic dye degradation activity against methylene blue (MB). Notable antibacterial activity in planktonic growth assays with inhibition zones of 6.15 mm and 6.9 mm and 63.51% reduction in bacterial proliferation at concentrations of 150 μg/mL and 175 μg/mL, respectively were observed for SP-AgNps. At 175 μg/mL, biofilm formation was also suppressed by 55.55% along with a pronounced reduction in bacterial motility. In addition, SP-AgNPs facilitated a maximum of 86% dye degradation efficiency adhering to pseudo-first-order kinetics with a rate constant of 0.01991 min⁻¹. These findings underscore the potential of SP-AgNPs as multifunctional silver nanoparticles with promising applications in both biomedical and environmental domains.

Keywords *Spondias pinnata*, Silver nanoparticles, Characterization, Antibiofilm, Dye degradation

Silver nanoparticles (AgNPs) have attracted considerable attention owing to their unique physical, chemical, and biological properties[1–3]. These include antimicrobial, wound healing, anticancer, and anti-inflammatory activities, as well as applications in water purification, biomedical imaging and diagnostics, drug delivery systems, agriculture, and cosmetics and personal care sectors[4–10]. However, despite their wide-ranging benefits, AgNPs are also associated with potential toxicity risks to human health and the environment[10]. Traditionally, physical and chemical methods have been extensively employed for AgNPs synthesis[1,2]. Many of these approaches, however, rely on toxic and hazardous chemical reagents, raising serious environmental and biocompatibility concerns[3,4]. Furthermore, residual chemical substances can adsorb onto the nanoparticle surfaces, thereby limiting their suitability especially in biomedical and pharmaceutical applications[2]. In contrast, phytochemical-mediated (phytogenic) synthesis of AgNPs offers an eco-friendly, sustainable, and cost-effective alternative, while often imparting enhanced physicochemical and biological potential to the nanoparticles[3–8]. Plant-derived phytomolecules such as terpenoids, flavonoids, amino acids, and carboxylic acids play a dual role by acting as both reducing agents – facilitating the conversion of metal ions and stabilizing agents, preventing agglomeration and imparting colloidal stability to the synthesized nanoparticles[3,6].

Biofilm formation by pathogenic bacteria is a major concern in both clinical and environmental settings. It is estimated that over 80% of chronic infections involve bacterial biofilms which resist conventional antibiotics[11–15]. Biofilm-associated infections present significant treatment challenges due to their structural resilience and antibiotic resistance, necessitating the development of advanced antimicrobial strategies[16–18]. Overcoming biofilm-related obstacles remains a critical focus in biomedical research, especially in the context of chronic infections and device-associated complications[19,20]. The ability of silver nanoparticles to inhibit biofilm

[1]Department of Chemistry, Tripura University, Suryamaninagar 799022, West Tripura, India. [2]Department of Chemistry, Iswar Chandra Vidyasagar College, Belonia 799155, South Tripura, India. [3]Department of Medical Laboratory Technology, Women's Polytechnic, Hapania 799130, Tripura, India. [4]Department of Physiology, University of Calcutta, Kolkata 700009, West Bengal, India. [5]Department of Physiology, Ananda Chandra College, Jalpaiguri 735101, West Bengal, India. ✉email: ucd1972@tripurauniv.ac.in

formation and reduce bacterial motility offers a promising approach to overcome biofilm-associated therapeutic challenges[20].

Escherichia coli (*E.coli*) is considered as one of the most virulent pathogens capable of inducing biofilm associated infections in humans[21,22]. With the rising tolerance of microbial infections to conventional drugs, advancements in medical interventions have increasingly focused on exploring nanoparticles positioning as a frontier area in microbiology. AgNPs a prominent focus of microbiological research, may play a vital role in the development of powerful antimicrobial agents with remarkable antibiofilm properties[21–24].

On the other hand, the textile industry is one of the largest consumers of water and chemicals, producing vast amounts of wastewater contaminated with synthetic dyes[25]. These dyes are often non-biodegradable, toxic, and resistant to conventional treatment methods posing serious environmental and health risks[26–29]. Catalytic dye degradation has emerged as an effective approach to manage this pollution and mitigate its impact. Methylene Blue (MB) is a synthetic dye widely used in the textile industry due to its vibrant blue color, ease of application, and compatibility with various fabric types[30]. It is commonly employed as a cationic (basic) dye for dyeing and printing processes, particularly for materials like cotton, silk, and wool[30,31]. The use of MB in the textile industry generates large volumes of dye-contaminated wastewater which poses significant environmental challenges because of its toxicity, non-biodegradability and aesthetic pollution of water bodies[31]. Catalytic dye degradation is a promising and sustainable solution for managing textile industry produced wastewater[28,29]. By harnessing advanced catalytic techniques and nanotechnology, the industry may significantly reduce its environmental footprint promoting cleaner production practices. Catalysts enhance the breakdown of complex dye molecules into less harmful or biodegradable components to reduce the toxic effects on aquatic ecosystems[28–30]. Nanoparticle based catalytic methods for dye degradation generally utilizes UV or visible lights to degrade dyes[26,27]. Moreover nanomaterials, particularly silver, gold, and iron oxide nanoparticles, have revolutionized catalytic dye degradation due to their enhanced catalytic activity, unique optical and electronic properties and sometimes their reusability[27,28]. A common method of dye degradation is the chemical breakdown of dyes using a reducing agent such as sodium borohydride ($NaBH_4$) which requires catalyst to speed up the reaction[27–30]. Silver nanoparticles have been proven to be one of the highly effective catalysts for this purpose[30,31]. However, their catalytic performance depends on the physicochemical nature viz. shape, size and caping or stabilizing agents of the nanoparticles[30,32].

Spondias pinnata (SP), commonly known as hog plum or Indian hog plum, is a tropical tree widely recognized in traditional medicine for its therapeutic properties[33]. Its bark is rich in bioactive compounds including tannins, saponins, alkaloids, and phenolics, which contribute to its diverse pharmacological activities[33–38]. Despite this phytochemical richness, the optimized synthesis and functional evaluation of silver nanoparticles conjugated with *S. pinnata* extract (SP-AgNPs) was not explored previously for microbial pathogenesis control or catalytic applications. In this context, the central hypothesis of this study was that the bioactive components of *S. pinnata* bark (SP bark) could act as both reducing and stabilizing agents in the green synthesis of silver nanoparticles with substantial antibacterial, antibiofilm, and catalytic properties to the resulting SP-AgNPs. The novelty of this work lies in the synthesis and multifunctional evaluation of SP-AgNPs, revealing their potential as dual-action agents for antimicrobial treatment and environmental remediation. Thus, this study significantly underscored its ecofriendly approach, use of a traditionally valued plant, and demonstration of long-term nanoparticle stability, paving the way for sustainable nanotechnology applications in biomedicine and wastewater treatment.

Materials and methods
Chemicals and reagents
All the reagents used in this work were of high analytical grade and used without further purification. Silver nitrate ($AgNO_3$, 99.9% Merck), Methylene Blue (MB, Merck), Sodium borohydride ($NaBH_4$, Merck) and Bacterial culture mediumviz. Luria-Bertani (LB) was obtained from Himedia (India). Bacterial strains such as *E. coli* MTCC 118 were purchased from IMTECH (Institute of Microbial Technology), a premier research institute dedicated to advancing microbial science and technology in India. All aqueous solutions used in this study were prepared using double-distilled (dd) water to ensure purity and consistency throughout the experimental procedures.

Collection, identification, and extraction of plant material
The *S. Pinnata* (Figure S1 in supplementary) bark was collected from Niharnagar (23º11′56.6′′ N 91º22′22.8′′E), a village of South Tripura district, India. The plant was identified and authenticated by a taxonomist from the Department of Botany, Tripura University, and a voucher specimen has been preserved in the departmental herbarium under the accession number TUH/4421. The collected bark of *S. pinnata* was thoroughly washed with water to remove surface impurities and then shade-dried at room temperature. The dried material was subsequently broken into small fragments and ground into a fine powder using a mechanical grinder. A quantity of 5 g of the powdered bark was mixed with 250 mL of double-distilled (dd) water in a round-bottom flask and heated in a water bath at 60 °C for 1 h. After cooling to room temperature, the mixture was filtered using Whatman No. 41 filter paper. The resulting filtrate was centrifuged at 5000 rpm for 20 min to remove residual particulates. The clear supernatant, coded as SP, was collected and stored at 4 °C in a refrigerator for further experimental uses.

Preparation of silver nanoparticles
As a preliminary experiment, 10 mL of aqueous *S. pinnata* bark extract (20 mg/mL) was mixed with 10 mL of 2 mM aqueous silver nitrate ($AgNO_3$) solution in an Erlenmeyer flask. The reaction mixture was continuously stirred at 400 rpm using a magnetic stirrer (IKA CMAG HS7) at ambient temperature (~ 25 °C). The initial indication of silver nanoparticle (Sp-AgNP) formation was observed through a gradual color change of the

reaction mixture from light yellow to reddish brown over time (Figure S2 in supplementary). The synthesis of SP-AgNPs was further confirmed by UV-Visible spectrophotometry, which revealed a characteristic surface plasmon resonance (SPR) peak at $\lambda_{max} = 430$ nm. Following nanoparticle formation, the solution was centrifuged at 5000 rpm for 15 min. The resulting pellet was washed thoroughly for five times with double-distilled water to remove unbound phytochemicals and residual impurities.

Optimization of SP-AgNPs synthesis
Optimization of SP extract to AgNO₃ ratio
10 ml SP bark extract (20 mg/ml) was mixed with 10 ml of $AgNO_3$ aqueous solution of different concentrations (0.5, 1, 2, 3, 4, and 5 mM) with constant stirring at room temperature for 3 h. The formation of the AgNPs was monitored using UV-VIS spectroscopy[10]. Optimum concentration of SP bark extract was determined by mixing SP extract to $AgNO_3$ in different ratios (v/v) such as 1:1, 1:2, 1:3, 1:4, 1:5 and 1:6 for each one of the concentrations. The ratio that showed most intense SPR peak was treated as optimised ratio and used for subsequent synthesis of SP-AgNPs as needed.

Optimization of pH in AgNPs synthesis
The effect of pH on the formation of SP-AgNPs was investigated at four different pH (5,7,9,11) with optimum concentration (3 mM) and mixing ratio (v/v 1:4) of SP extract to $AgNO_3$. The pH of the solution was maintained by using 0.1 N hydrochloric acid (HCl) and 0.1 N sodium hydroxide (NaOH)[10].

Optimization of reaction temperature
After having optimum mixing ratio of SP bark extract to $AgNO_3$ solution, optimum concentration and optimum pH (9), reaction was studied within temperature ranges from ambient to 100 °C to find the optimum temperature for SP-AgNPs synthesis[10].

Optimization of reaction time
After having optimum mixing ratio (SP bark extract to $AgNO_3$ solution), optimum concentration and optimum pH in hand, optimization of reaction time of SP-AgNPs synthesis was carried out at room temperature (optimised) by mixing $AgNO_3$ with SP extract at optimized ratio. After regular time intervals, aliquots were taken and the formation of SP-AgNPs was monitored using UV-VIS spectroscopy[10].

Identification and characterization of SP-AgNPs
Identification of SP-AgNPs was done by UV-Visible scanning (Shimadzu UV-2600i) while characterizations were completed by using TEM (JEM-2100, 200 kV, Jeol), FESEM (ZEISS, sigma 300), XRD (Bruker AXS, D8), XPS (Thermo Fischer Scientific, K alpha), ICPOES (Thermo scientific iCAP 7600), FTIR (Bruker Alpha II) analyses as well as Zeta potential measurement and DLS studies (Anton Paar Litesizer 500). The stability, surface charge and size distribution of the SP-AgNPs were also predicted by Zeta potential and DLS studies. The concentration of SP-AgNPs was determined by ICPOES study. Qualitative functional groups analysis in the plant extract and SP-AgNPs were done by FTIR analysis. The shape, size and aggregation features were studied by TEM, FESEM and XRD. TEM-EDX and XPS studies also conducted for elemental composition of the SP-AgNPs[3].

Catalytic degradation of methylene blue dye
To assess the catalytic activity of the SP-AgNPs, the degradation of MB dye was carried out in the presence of $NaBH_4$[30–32]. In brief, a conical flask was successively charged with 50 mL of methylene blue solution of 10 ppm concentration, 2 mg of sodium borohydride and 2 mg of SP-AgNPs. The mixture was continuously stirred at room temperature and absorption (λ_{max} for MB at 662 nm) was measured at various time intervals using UV spectrophotometer. A similar experiment was conducted without adding SP-AgNPs for reference λ_{max} values of MB dye[30–32]. Pseudo first-order kinetics was considered to evaluate the apparent rate constant using the following Eq.

$$\ln\left(\frac{A_t}{A_0}\right) = -kt \tag{1}$$

In addition, percentage of dye degradation was estimated with the following equation.

$$Percent\ of\ degradation = \frac{(A_0 - A_t)}{A_0} \times 100 \tag{2}$$

Where, A_0 is the initial absorbance of dye, A_t is the absorbance of the dye at time t and k is the rate constant.

Microbial strains and growth media
In the present work, *E. coli* strain (MTCC 118) was cultured in Luria Bertani broth (LB) media. Initially bacteria were streaked from a −80 °C glycerol stock onto LB agar plate and a fresh single colony was inoculated into 25 ml media and incubated at 37 °C for 24 h. Aliquots of 10^6 CFU/mL bacterial cell suspensions were used for all subsequent experiments[39,40].

Antimicrobial susceptibility testing
Disc diffusion method using the Bauer-Kirby technique was employed for determination of microbial growth inhibition zone as per recommendation of National Committee for Clinical Laboratory Standards (NCCLS).

In brief, paper discs of 4 mm diameter soaked separately in SP-AgNPs, AgNO₃, *S. pinnata* bark extract and gentamicin (standard antibiotic) solutions of various concentrations, placed on plates overlaid with soft agar (0.7%) with previous inoculation of *E. coli* and subsequently incubated at 37 °C for 48 h. The size of the clear zone around the disc was measured to determine the inhibition considering the values as zone of inhibition. Minimum inhibitory concentration (MIC) of SP-AgNPs against *E. coli* was also determined using standard broth micro dilution assay[39,40].

Evaluation of *E. coli* biofilm formation

E. coli was grown in 96-well plate containing LB medium and incubated at 37 °C for 48 h. Wells were then washed three times with sterile Phosphate Buffer Saline (PBS) and stained with 0.1% (v/v) safranin. The excess stain was removed by washing again with sterile PBS and kept overnight for drying at 37 °C. Stain adherent with bacteria were re-dissolved in dimethyl sulfoxide (DMSO) and absorbance was recorded at 492 nm[39,40].

Motility analysis of *E. coli* under treatment of SP-AgNPs

Sliding motility of *E. coli* and its modulation under the treatment of SP-AgNPs were tested through their ability to spread on LB soft agar media (Himedia, India) from the point of inoculation. Briefly, aliquots of bacteria (~ 10⁶ CFU/ml) were spot inoculated in the centre of petri dishes charged with 2.4 g/l nutrient agar media and treated with sub-inhibitory doses of SP-AgNPs. Dishes were dried for 20 min at room temperature and then incubated at 37 °C for 48 h. Colony growth expansions from the point of inoculation were recorded[39,40].

Antibiofilm activity of SP-AgNPs

Anti-biofilm potentiality of SP-AgNPs against *E. coli* was evaluated by repeating the method described in Sect. "Evaluation of *E. coli* biofilm formation". In short, *E. coli* bacteria were allowed to grow with sub-MIC doses of SP-AgNPs and without SP-AgNPs in parallel. After all the necessary follow up steps, absorbances of both the parallel bacterial growth stained with safranin were measured at 492 nm[39,40]. Percentage of *E. coli* biofilm inhibition was determined using the following formula:

$$\text{Biofilm Inhibition } (\%) = \frac{\{(\text{OD of NP untreated } E.coli \text{ growth}) - (\text{OD of NP treated } E.coli \text{ growth}\}}{(\text{OD of NP untreated } E.coli \text{ growth})} \times 100$$

Microbial adherence studies on glass surface by fluorescent microscope

A sterile cover slip was placed in 35 mm petri dish and the *E. coli* biofilm were allowed to form. Cover slips with biofilm were then incubated with a fluorescent dye viz. acridine orange in dark and fluorescent was measured using i3 filter under fluorescent microscope. Images were captured from 20 different fields from a single cover slip and best representative images were produced[39,40].

Statistical analysis

All the biological experiments were performed in triplicate and observed data were recorded as the mean ± standard deviation. Significance were determined by using one way ANOVA t-test and mentioned as P value < 0.01 (noted with*), P value < 0.001 (noted with**) and P value < 0.0001 (noted with***).

Results

Synthesis and stability of SP-AgNPs

Biogenic SP-AgNPs were synthesised by using SP bark extract and found significantly stable for 6 ~ 7 months at normal temperature (25 ± 4 °C). The stability of SP-AgNPs was supported by the negative zeta potential value. The repulsive forces between negatively charged SP-AgNPs are likely to play the key role against the aggregation of the nanoparticles[41].

Optimization of SP-AgNPs synthesis

The optimal synthetic conditions of SP-AgNPs were achieved by optimizing various factors viz. concentrations of the reactants, mixing ratio of the reactants, pH of the reaction mixture, temperature and reaction time. Formation and qualitative quantification of SP-AgNPs was monitored by measuring the characteristic absorbance at SPR band (λ_{max} 439 nm) using a UV–VIS spectrophotometer (Fig. 1).

Optimum ratio of SP extract to AgNO₃
The optimum mixing ratio (Fig. 1B) of AgNO₃ to SP bark extract to yield the maximum amount of nanoparticles was determined to be 1:4 (v/v) for the synthesis of SP-AgNPs.
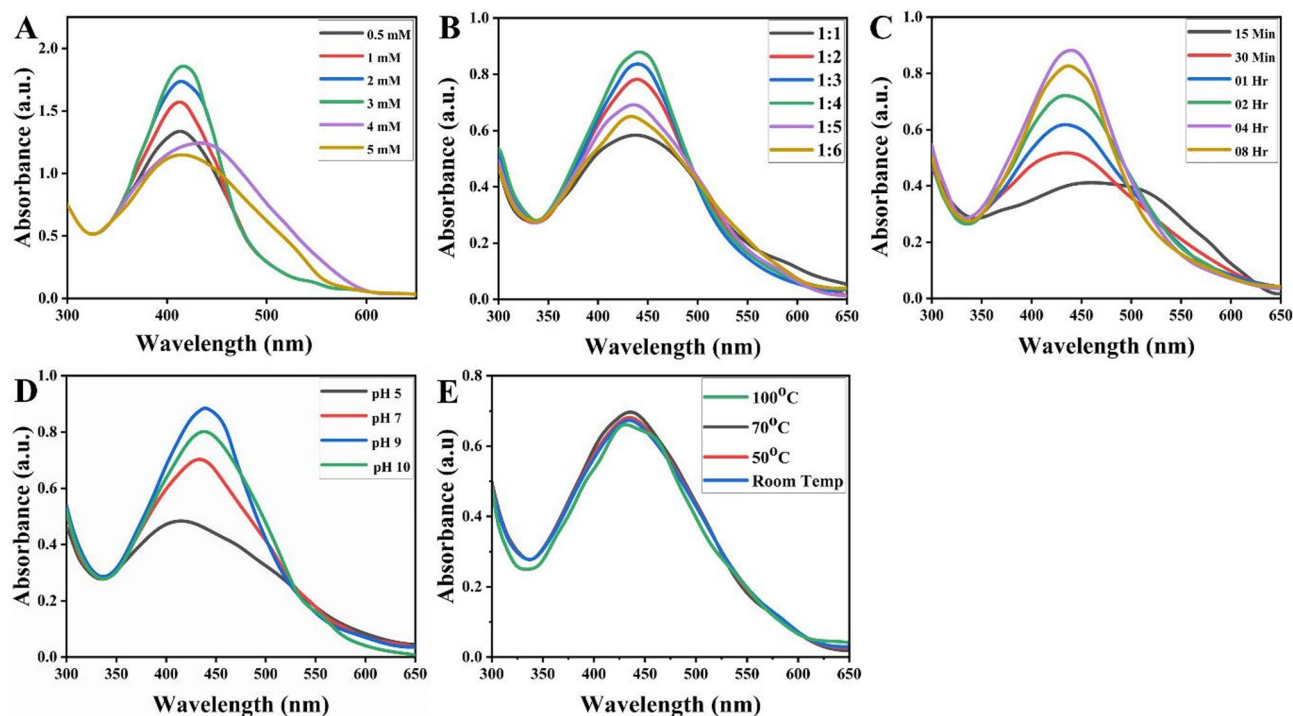
Optimum concentration of AgNO₃
The optimum concentration of AgNO₃ was determined by mixing of SP bark extract (20 mg/ml) with increasing concentration of AgNO₃ at previously optimized ratio. It was observed that AgNO₃ solution of 3mM concentration was optimum concentration for the synthesis of SP-AgNPs indicated by highest intense SPR peak at λ_{max} 439 nm (Fig. 1A).

Optimization of pH
Aqueous extract of SP bark exhibited pH 5.9. So in optimization process, the reaction was studied within the range of pH viz. 5–11 i.e. little lower than pure extract to a moderately higher level. It was observed that at pH 9, the reaction mixture exhibited maximum absorbance (Fig. 1C) at the characteristics SPR peak (439 nm) confirming this as the optimum pH value for the synthesis of SP-AgNPs.

Fig. 1. Optimization of various reaction parameters on the synthesis of SP-AgNPs, (**A**) AgNO$_3$ concentration (**B**) Ratio of AgNO$_3$ conc. and SP extract (**C**) Reaction time (**D**) Reaction medium pH (**E**) Reaction temperature.

Optimization of reaction temperature
Temperature optimization study for the SP-AgNPs synthesis revealed (Fig. 1E) that there was no significant increase of SP-AgNPs concentration within the temperature range of ambient to 100 °C instead a little decrease of concentration was observed. So, the ambient temperature (~ 25 °C) was considered as the optimum temperature for SP-AgNPs synthesis.

Optimization of reaction time
Time optimization experimental results (Fig. 1D) showed that the formation of SP-AgNPs at room temperature was maximum at 60 min and thus considered as the optimum reaction time for the synthesis of SP-AgNPs.

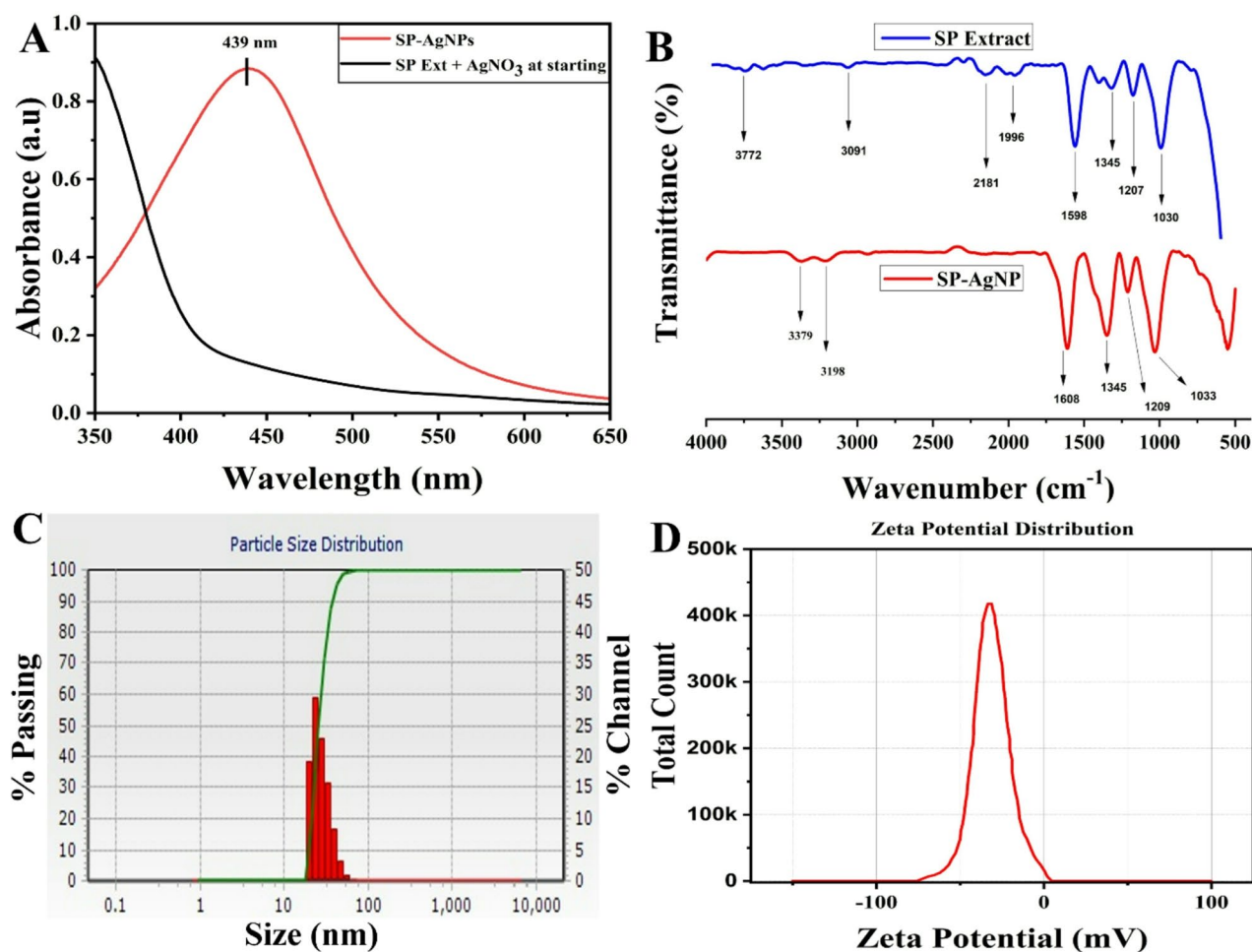## Characterisation of nanoparticles
UV-VIS study
The optical features of metal nanoparticles are the most important features for their characterization which varies according to the size to volume ratio of the particles. Silver nano particles (AgNPs) typically has a central peak (λ_{max}) between 350 and 450 nm. The initial UV-VIS scanning (300–600 nm) of SP-AgNPs showed the characteristic SPR band at the wavelength (λ_{max}) of approximately 439 nm confirming the formation of SP-AgNPs in the solution. (Fig. 2A).

Fourier transform infrared spectroscopy (FTIR) study
FTIR spectroscopy was used to identify the functional groups in SP bark extract involved in reduction of silver ions and subsequent stabilization of SP-AgNPs[3,42–45]. FTIR spectra (Fig. 2B) of both the plant extract and the SP-AgNPs showed key peaks at 3772 cm^{-1} (-OH, -NH stretching), 3091 cm^{-1} (aromatic C-H stretching), 2181 cm^{-1} (C≡C or C≡N stretching), and 1598 cm^{-1} (C=C aromatic stretching) indicating the presence of phytochemicals having these type of groups/bonds. Additional peaks at 1345 cm^{-1}, 1207 cm^{-1}, and 1030 cm^{-1} may be due to C-H bending and C-O stretching frequencies of most likely phytoconstituent such as phenolic compounds, proteins, or polysaccharides. Besides, SP-AgNPs IR spectrum (Fig. 2B) showedsome peaks shifting in association with intensity changes compared to the pure SP-extract. It was an indication of the involvement of chemical constituents present in SP bark extracts both in reduction of silver ions during synthesis and subsequent capping of the SP-AgNPs.

DLS and zeta potential study of SP-AgNPs
Dynamic light scattering (DLS) is an effective method for characterizing nanoparticle in terms of surface charge, size distribution, and overall quality of nanoparticles[46,47]. Outcome of this studies (Fig. 2C) demonstrated the size distribution of SP-AgNPs ranged from 10 to 100 nm. The size distribution display of a single peak indicated

Fig. 2. Spectroscopic analysis (**A**) UV-Spectra of SP-AgNPs showing SPR peak at 439 nm. (**B**) FTIR spectra of SP extract and SP-AgNPs. (**C**) DLS of SP-AgNPs. (**D**) The Zeta potential of SP-AgNPs.

the mono-dispersed production of SP-AgNPs. The zeta potential value of SP-AgNPs was found as −37 mV indicating the formation of highly stable negatively charged nanoparticles (Fig. 2D).

TEM and FE-SEM imaging of SP-AgNPs
SP-AgNPs average size was determined as 32±5 nm (Fig. 3A) from their TEM analysis. The histogram derived from TEM data resulted the particles diameter ranging from 27 nm to 37 nm, with an average area of approximately 1100 nm² (Fig. 3B). Face-centered cubic (fcc) lattice arrangement of the SP-AgNPs was established from the ring pattern in SAED image (Fig. 4B). FE-SEM captured images of SP-AgNPs (Fig. 3C) reliably confirmed the spherical shape and uniform distribution of SP-AgNPs[47–49].
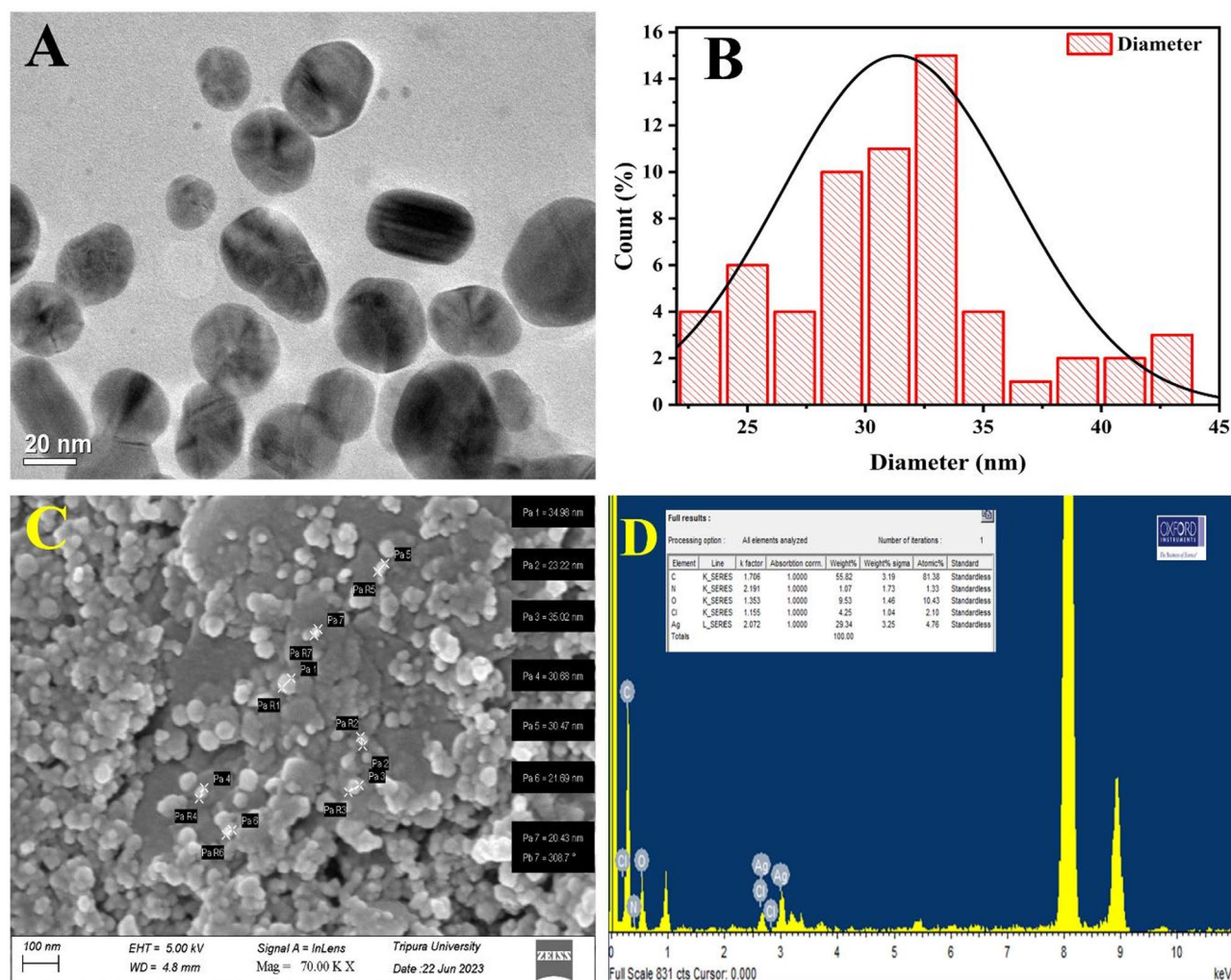
Energy dispersive X-ray study of SP-AgNPs
Energy Dispersive X-ray (EDX) studies for purity assessment and elemental composition of SP-AgNPs confirmed the presence of 55.82% C, 29.34% Ag, 9.53% O, 4.25% Cl, and 1.07% N (Fig. 3D). The presence of peaks at 3 keV and 3.2 keV indicated the complete reduction of the silver ions[47,48].

X-ray diffraction study of SP-AgNPs
Powder XRD diffraction pattern of SP-AgNPs showed peaks at 38.07°, 44.16°, 64.39°, and 77.26° corresponding to the 111, 200, 220, and 311 lattice planes, respectively (Fig. 4A). Presence of these lattice planes favoured fcc arrangements of SP-AgNPs as per the ICDD PDF2 (No. 071-4613) database. The average size of the crystalline SP-AgNPs was found to be approximately 37 nm as calculated using the Scherrer formula[47,48].

X-ray photoelectron spectroscopy (XPS) study of SP-AgNPs
X-ray photoelectron spectroscopy (XPS) analysis of SP-AgNPs revealed three prominent peaks (Fig. 5A-D) corresponding to the binding energy regions of 532.4 eV (O 1s), 285.24 eV (C 1s), and 368.2 eV (Ag 3d), indicating the chemical composition of the SP-AgNPs. The elemental composition was found to be 3.55% Ag, 54.31% C, and 36.81% O. The relatively higher percentages of carbon and oxygen compared to silver are

Fig. 3. Electron microscopic characterization (**A**) HR TEM image of SP-AgNPs showing spherical shape of the nanoparticle. (**B**) Histogram of the diameter of SP-AgNPs in which the average diameter is 32 nm (**C**). FESEM image of SP-AgNPs. (**D**) TEM-EDX of SP-AgNPs.

attributed to the abundance of organic phytomolecules acting as capping agents on the nanoparticle surface. Furthermore, XPS provides surface-sensitive information within a depth of approximately 10 nm, where these phytomolecules are concentrated, while the silver atoms are embedded deeper in the core of the nanoparticles. This surface localization explains the relatively lower atomic percentage of silver detected[3,43,47,48]. The high-resolution XPS spectrum of SP-AgNPs (Fig. 5C) displays two distinct peaks at 368.2 eV and 374.4 eV, which correspond to the spin-orbit components of Ag $3d^{5/2}$ and Ag $3d^{3/2}$, respectively, confirming the presence of metallic silver (Ag^0)[3,43,46,47].

ICP-OES study of SP-AgNPs
ICP-OES analysis revealed that the silver concentration in SP-AgNPs was 28.137 ppm, determined using a calibration curve prepared from a standard AgNPs solution at an operative wavelength of 328.068 nm, with a limit of detection (LOD) of 0.0150 ppm.
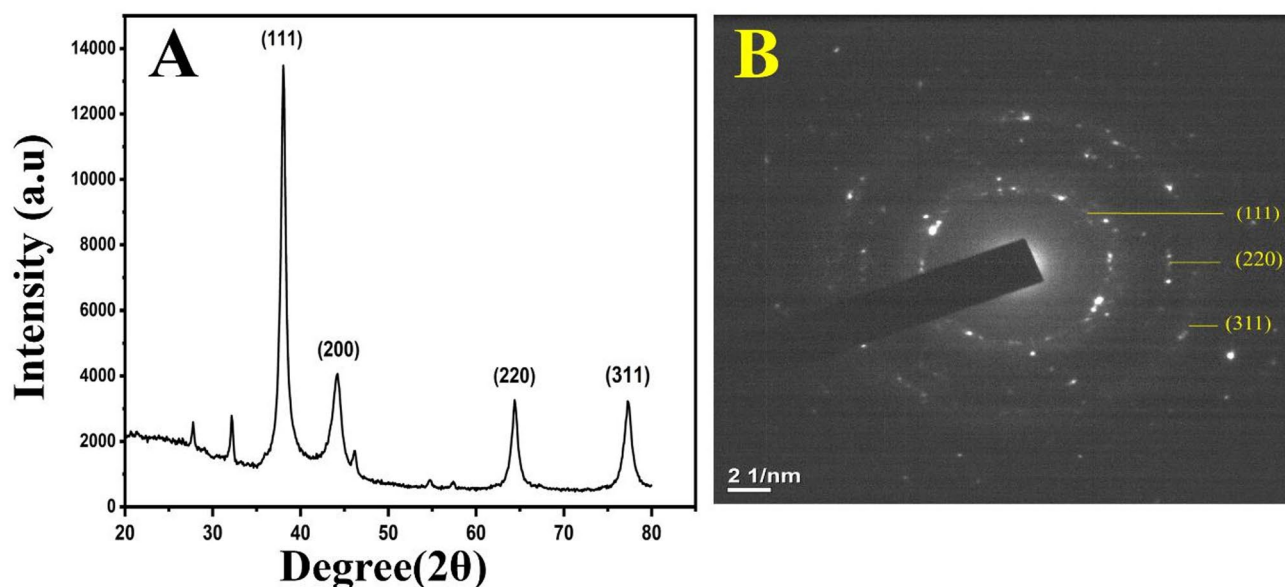
MB dye degradation by SP-AgNPs
The catalytic dye degradation efficacy of the biogenic SP-AgNPs was evaluated through $NaBH_4$-mediated chemical reduction of methylene blue (MB) by titrimetric UV–VIS absorption spectroscopy[32,50–57]. A maximum of 86% degradation of MB was achieved in the presence of SP-AgNPs as indicated by the significant decrease in absorbance at 662 nm, the λ_{max} of MB (Fig. 6A-D). The reaction followed pseudo-first-order kinetics, with a calculated rate constant (k) of 0.01991 min^{-1}.

Antibacterial effect of SP-AgNP on planktonic form of *E. coli*
The antibacterial efficacy of SP-AgNPs against *E. coli* was assessed by evaluating their impact on planktonic bacterial growth[21–24]. At concentrations of 150 µg/mL and 175 µg/mL, SP-AgNPs exhibited 63.51% inhibition, with zone of inhibition (ZOI) diameters of 6.15 mm and 6.9 mm, respectively (Fig. 7A). In comparison, the

Fig. 4. (**A**) PXRD of SP-AgNPs. (**B**) SAED image of SP-AgNPs.

standard antibiotic gentamicin demonstrated a maximum inhibition of 98.93%, with a ZOI of 7.8 mm at a significantly lower concentration of 1.25 µg/mL (Fig. 7A). Furthermore, a comparative analysis of the individual components (Fig. 7B) revealed that the plant extract (S. pinnata) alone exhibited no inhibitory activity, even at a concentration of 175 µg/mL. AgNO₃, on the other hand, showed a ZOI of 5.4 mm at the same concentration. In contrast, SP-AgNPs demonstrated significantly larger inhibition zones of 6.15 mm and 6.9 mm at 150 µg/ mL and 175 µg/mL, respectively, under identical conditions (Fig. 7C). These findings clearly highlight the enhanced antibacterial activity of biosynthesized SP-AgNPs compared to both the plant extract and AgNO₃ alone, emphasizing the synergistic effect of silver nanoparticles and phytochemicals derived from *S. pinnata* bark extract in generating potent antibacterial agents.

Antibiofilm effect of SP-AgNPs on *E. coli* biofilm

The antibiofilm efficacy of SP-AgNPs was evaluated against *E. coli*, revealing a substantial biofilm attenuation of 55.55% at a concentration of 175 µg/mL. In comparison, the standard antibiotic gentamicin demonstrated 94.44% biofilm inhibition at a significantly lower sub-inhibitory concentration of 1.25 µg/mL (Fig. 8A), indicating the notable antibiofilm potential of SP-AgNPs. In addition, SP-AgNPs markedly reduced the motility of *E. coli* at the same concentration (175 µg/mL), as shown in the motility assay (Fig. 8B). Further confirmation was provided by fluorescence microscopy, which revealed a considerable reduction in bacterial aggregation upon SP-AgNP treatment, thereby corroborating its biofilm inhibition capacity against *E. coli* (Fig. 9).

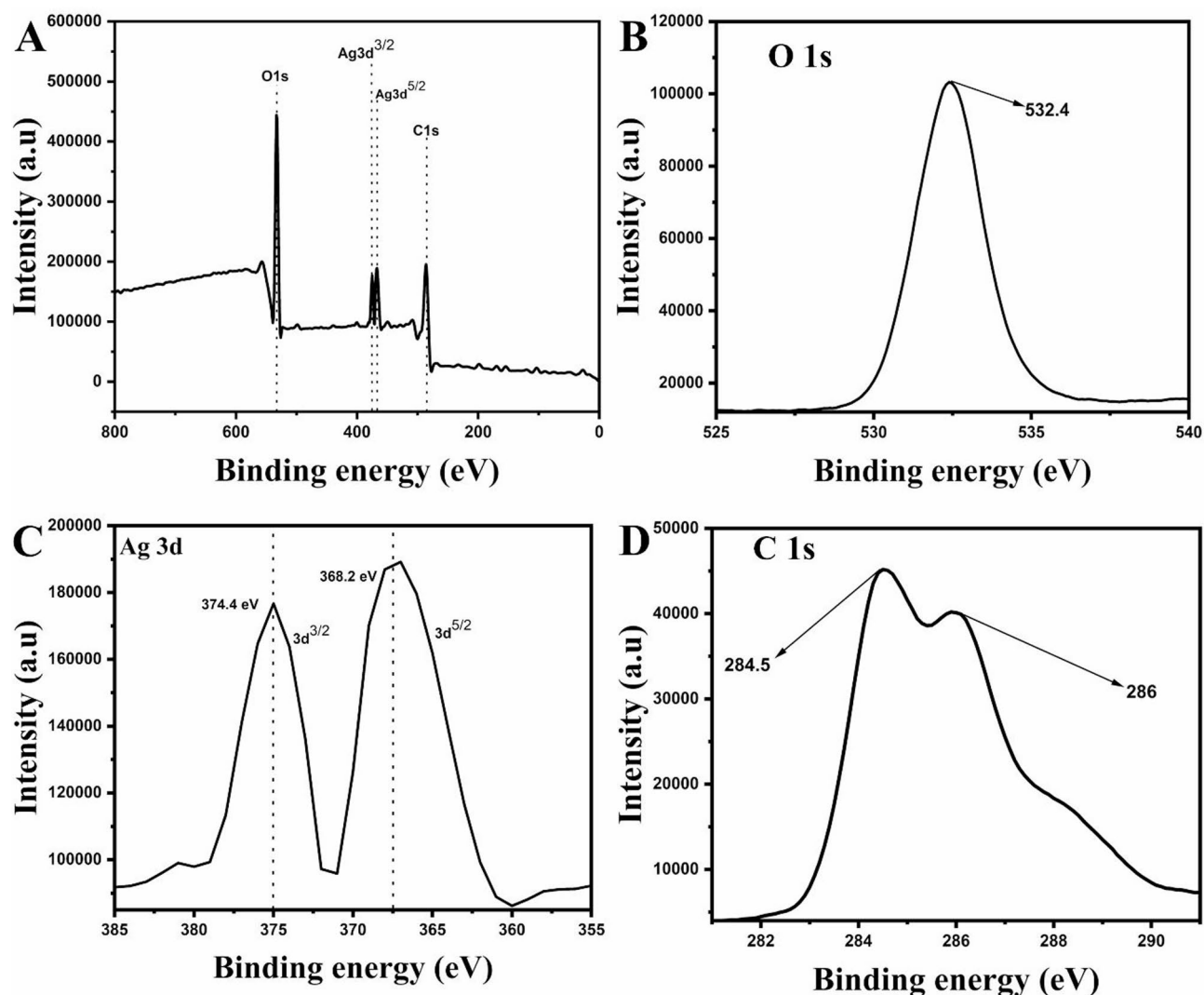### Effect of SP-AgNPs on bacterial motility

In the motility assay, SP-AgNPs exhibited a significant reduction in bacterial motility compared to the untreated control (Fig. 8B). Furthermore, it was observed that bacterial colonization was markedly disrupted in the presence of SP-AgNPs, reinforcing their potential to inhibit biofilm development by interfering with the initial adhesion and aggregation processes.

Discussion

Silver nanoparticles are highly versatile nanomaterials appreciated for their distinctive physical, chemical, and biological characteristics[58,59]. Their wide array of applications spans across the field of drug discovery and development, biotechnology, catalysis, electronics, and environmental remediation[4,11,27–32,52–58]. However, traditional methods of synthesizing AgNPs often involve the use of toxic chemicals, high energy consumption, and the generation of hazardous by-products. Therefore, there is a pressing need to develop eco-friendly, cost-effective, and sustainable approaches to AgNP production. Green synthesis of AgNPs offers a promising solution by utilizing natural sources such as plants, microorganisms, or other biomolecules as both reducing and stabilizing agents. Among these, plant extracts, in particular, have emerged as a convenient method due to several advantages like ready availability, economic viability, easy handling, environmental friendliness, and having no yield of harmful by-products etc[3–6,8,9].

The green synthesis of silver nanoparticles (AgNPs) using *S. pinnata* bark extract involves the bioreduction of silver ions (Ag⁺) to elemental silver (Ag⁰) mediated by the phytochemicals present in the extract. Flavonoids and phenolic compounds, known for their high reducing ability, act as natural reducing agents by donating electrons to convert Ag⁺ into Ag⁰[36,38]. The reduced silver atoms initiate nucleation, forming small nanoparticle seeds, followed by the growth phase, during which additional Ag⁰ atoms deposit on these seeds, leading to the formation of stable silver nanoparticles. In addition to reduction, various other biomolecules such as tannins,
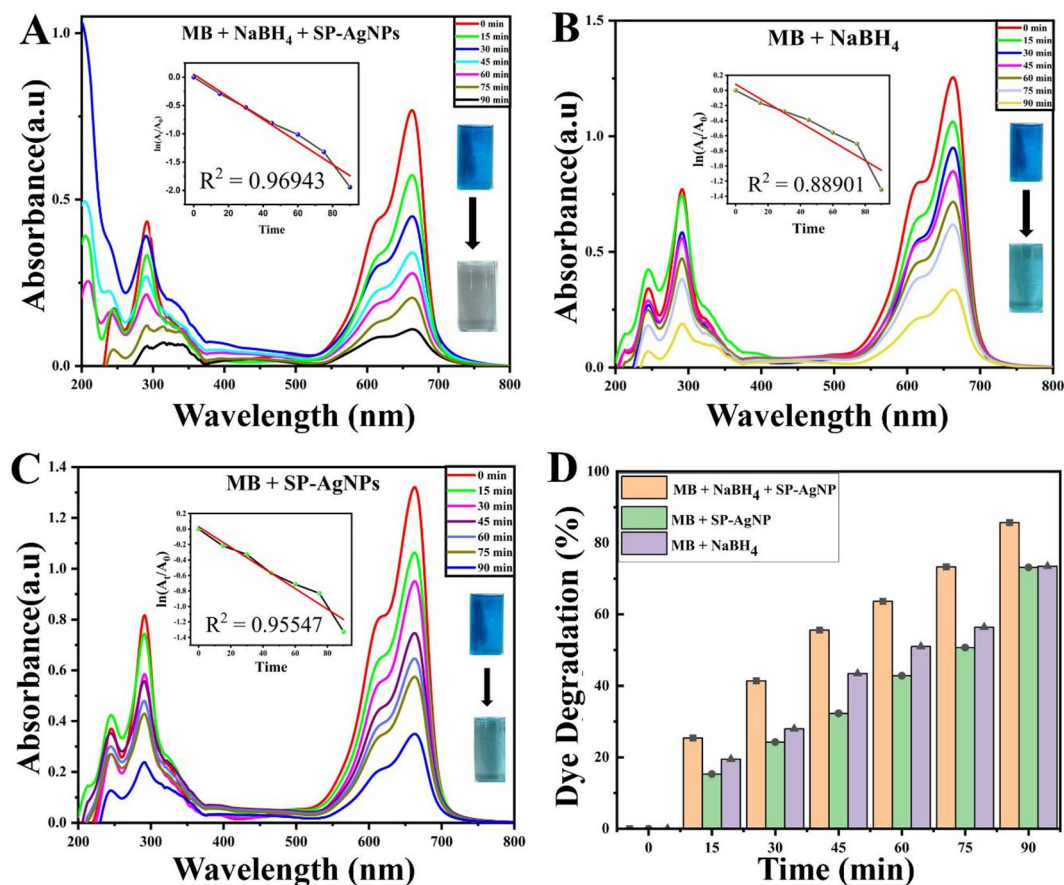
Fig. 5. XPS high-resolution spectra of SP-AgNPs (**A**) survey spectrum, (**B**) O 1 s orbital, (**C**) Ag 3 d orbital, and (**D**) C 1 s orbital.

saponins, amino acids, and other plant-derived metabolites functioned as capping and stabilizing agents. These molecules adsorb onto the surface of the nanoparticles, providing steric and electrostatic stabilization, thereby preventing agglomeration. This eco-friendly synthesis route eliminates the need for hazardous reducing or stabilizing chemicals and imparts additional biological functionalities to the nanoparticles through the presence of bioactive natural capping agents derived from *S. pinnata*[33–38].

In the wet-laboratory synthesis of silver nanoparticles using *S. pinnata* bark extract (SP-AgNPs), an initial visual indication of nanoparticle formation was the color change of the reaction mixture from light yellow to reddish brown. This chromatic shift is attributed to the excitation of surface plasmon resonance (SPR), a phenomenon characteristic of silver nanoparticles. The formation was further validated by UV-VIS spectrophotometric analysis, which revealed a distinct SPR band at 439 nm (λ_{max})[2–6]. The UV–VIS spectra of SP-AgNPs were compared to those of $AgNO_3$ and plant extract alone, both of which did not show any SPR peak in the 400–450 nm region, confirming that the observed 439 nm peak arises solely due to the formation of silver nanoparticles (Fig. 2A).

The SPR band of silver nanoparticles is highly sensitive to particle size, shape, dielectric environment, and capping agents[2–4]. In this study, a narrow and symmetric SPR peak was observed at 439 nm which suggested the formation of spherical SP-AgNPs with uniform size distribution[1–4]. However, time-resolved UV–Vis measurements showed a gradual increase in SPR intensity with incubation time, indicating a steady nucleation and growth process of SP-AgNPs. The absorbance at 439 nm was plateaued after 60 min of reaction suggesting the completion of maximum nanoparticle formation.

To ensure maximum yield and stability, various reaction parameters viz. $AgNO_3$ concentration, SP-extract concentration, mixing volume ratio of $AgNO_3$ to SP-extract, reaction time, pH of the reaction medium and reaction temperature were systematically optimized. The optimal conditions for the synthesis of SP-AgNPs were established by mixing a 3 mM aqueous solution of $AgNO_3$ with *S. pinnata* bark extract (20 mg/mL) in a 1:4
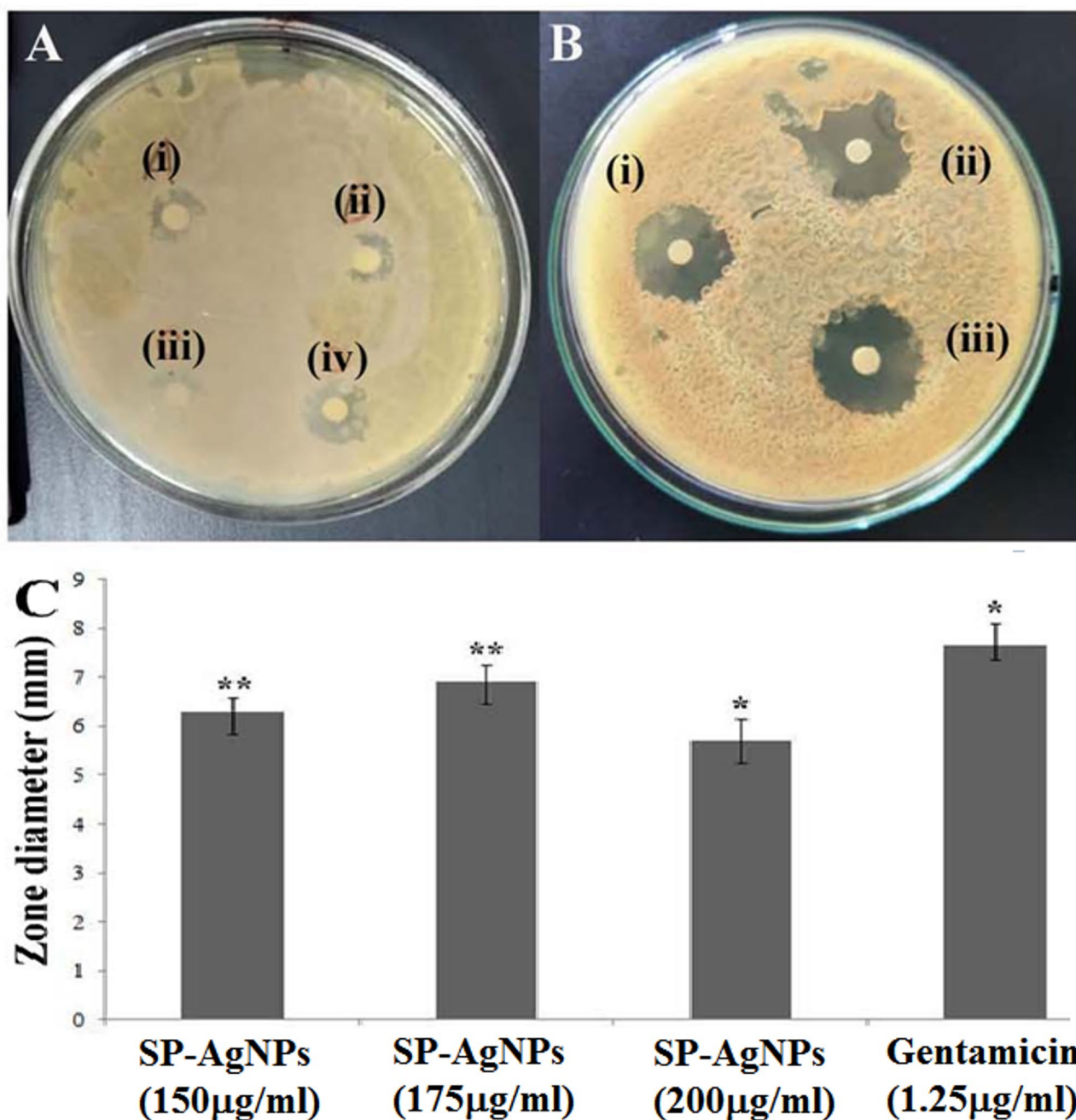
Fig. 6. Degradation of methylene blue (**A**) In presence of methylene blue (MB), Sodium borohydride (NaBH$_4$) and SP-AgNPs (**B**) In presence of methylene blue (MB) and Sodium borohydride (NaBH$_4$) (**C**) In presence of methylene blue (MB) and SP-AgNPs (**D**) Bar diagram to show comparative degradation percentages.

volume ratio, followed by constant stirring for 60 min at room temperature, while maintaining the reaction pH at approximately 9. Although room temperature (~25 °C) was effective, elevated temperatures (40–60 °C) led to faster reduction but resulted in broader SPR peaks, possibly due to particle aggregation. Thus, ambient temperature was selected for optimal balance between reaction speed and particle quality.

FTIR analysis of *S. pinnata* bark extract and SP-AgNPs (Fig. 2B) revealed significant changes in functional group characteristics, confirming the involvement of biomolecules from the extract in the reduction and stabilization of silver nanoparticles. In the IR spectrum of the parent *S. pinnata* extract, prominent absorption bands were observed at 3772 cm⁻¹, corresponding to –OH and –NH stretching vibrations, and at 3091 cm⁻¹, indicative of aromatic C–H stretching. These features suggest the presence of phenols, flavonoids, and proteins, which are well-documented for their reducing and capping abilities in green nanoparticle synthesis. Following nanoparticle formation, the FTIR spectrum of SP-AgNPs showed shifts and intensity changes in these characteristic peaks (Fig. 2B), indicating the active participation of hydroxyl/amine functional groups, likely derived from phenolic compounds and amino acids/proteins, in both the reduction of Ag⁺ ions to Ag⁰ and subsequent nanoparticle stabilization. Additionally, notable peak shifts were also observed at 1345 cm⁻¹, 1209 cm⁻¹, and 1033 cm⁻¹, which correspond to C–H bending, and C–O stretching/bending vibrations associated with carboxylic acids, esters, and polysaccharides. These shifts further suggest the involvement of carboxylate and ether-containing biomolecules, such as flavonoids, polysaccharides, and organic acids, in the capping and surface functionalization of the SP-AgNPs[2–6,10].

Dynamic Light Scattering (DLS) is a widely used technique for determining the particle size distribution of nanoparticles in suspension. It provides insights into the hydrodynamic diameter of nanoparticles by analyzing the fluctuations in light scattering intensity caused by the Brownian motion of particles in the medium. These fluctuations are influenced by particle size, surface charge, and interaction with the surrounding solvent[46,47]. In this study, DLS analysis of the synthesized SP-AgNPs revealed a size distribution ranging from 10 to 100 nm, with an average hydrodynamic diameter of approximately 40–45 nm. The relatively narrow distribution indicates a monodisperse suspension, suggesting efficient stabilization by the phytochemical capping agents derived from the *S. pinnata* bark extract.

Zeta potential analysis is a critical technique for evaluating the surface charge of nanoparticles in a colloidal dispersion, providing key insights into their stability and aggregation behavior. It measures the electrokinetic potential at the slipping plane between the nanoparticle surface and the surrounding medium, thereby indicating
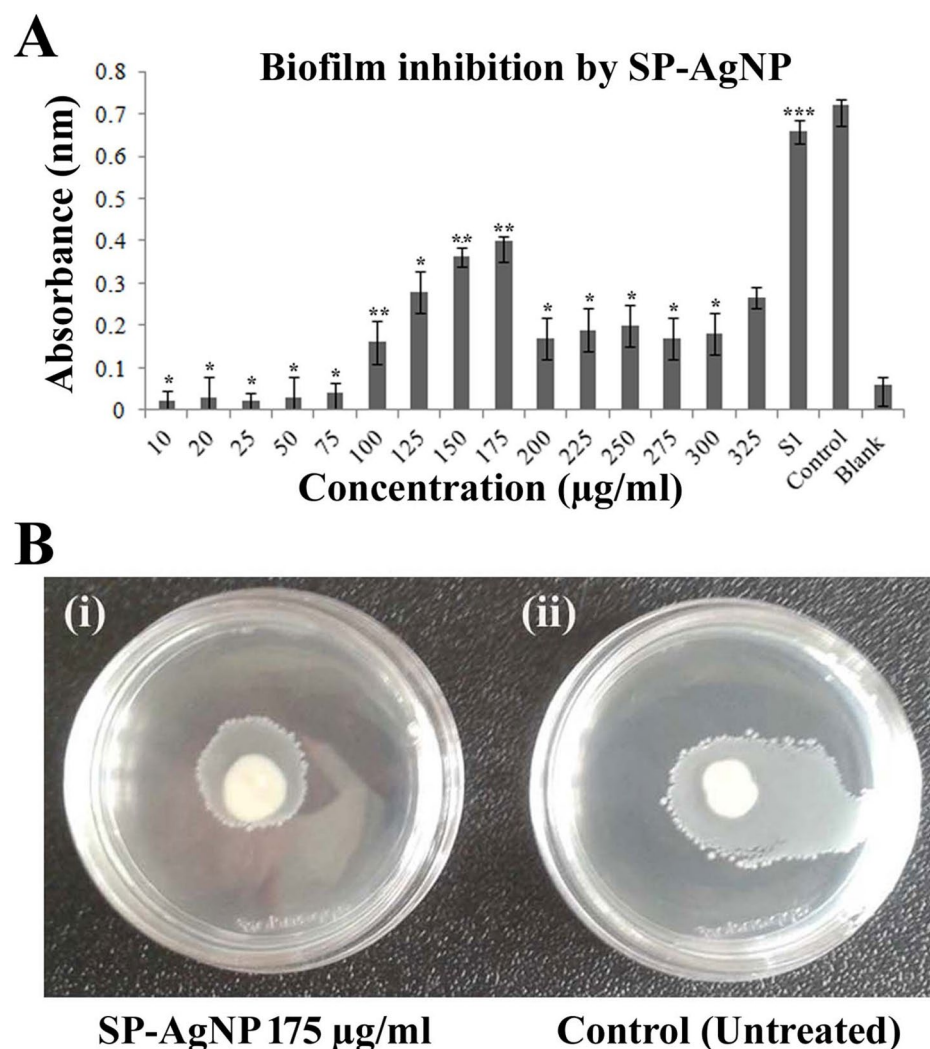
Fig. 7. Zone of inhibition of *E. coli* (**A**). (i) 150 μg/ml SP-AgNP (ii) 175 μg/ml SP-AgNP (iii) 200 μg/ml SP-AgNP (iv) gentamicin (**B**). (i) AgNO$_3$ solution (ii) SP-AgNP at 150 μg/ml B(iii)] gentamicin (**B**). Comparative Zone inhibition diameters of SP-AgNPs and gentamicin against *E. coli*.

how well nanoparticles are dispersed in a solution[41,46,47]. Typically, nanoparticles with zeta potential values greater than ± 30 mV exhibit strong electrostatic repulsion, which helps prevent agglomeration and promotes colloidal stability. In this study, the SP-AgNPs exhibited a zeta potential of −37 mV, confirming their high surface charge and excellent stability in aqueous suspension. This strong negative potential is likely due to the presence of anionic phytochemicals (e.g., phenolics, carboxylates) adsorbed on the nanoparticle surface, which also contribute to their steric and electrostatic stabilization.

The size, morphology, and surface characteristics of nanoscale particles are typically examined using high-resolution imaging techniques such as Transmission Electron Microscopy (TEM) and Field Emission Scanning Electron Microscopy (FESEM)[44,47]. In this study, TEM analysis of SP-AgNPs confirmed their spherical morphology and crystalline nature, with an average particle diameter of 32 ± 5 nm, as shown in Fig. 1A. The particle size distribution histogram derived from TEM images indicated that the majority of SP-AgNPs had diameters ranging from 27 to 37 nm, with an average projected area of approximately 1100 nm² (Fig. 3A, B). Furthermore, FESEM analysis supported the TEM findings, also revealing spherical-shaped nanoparticles
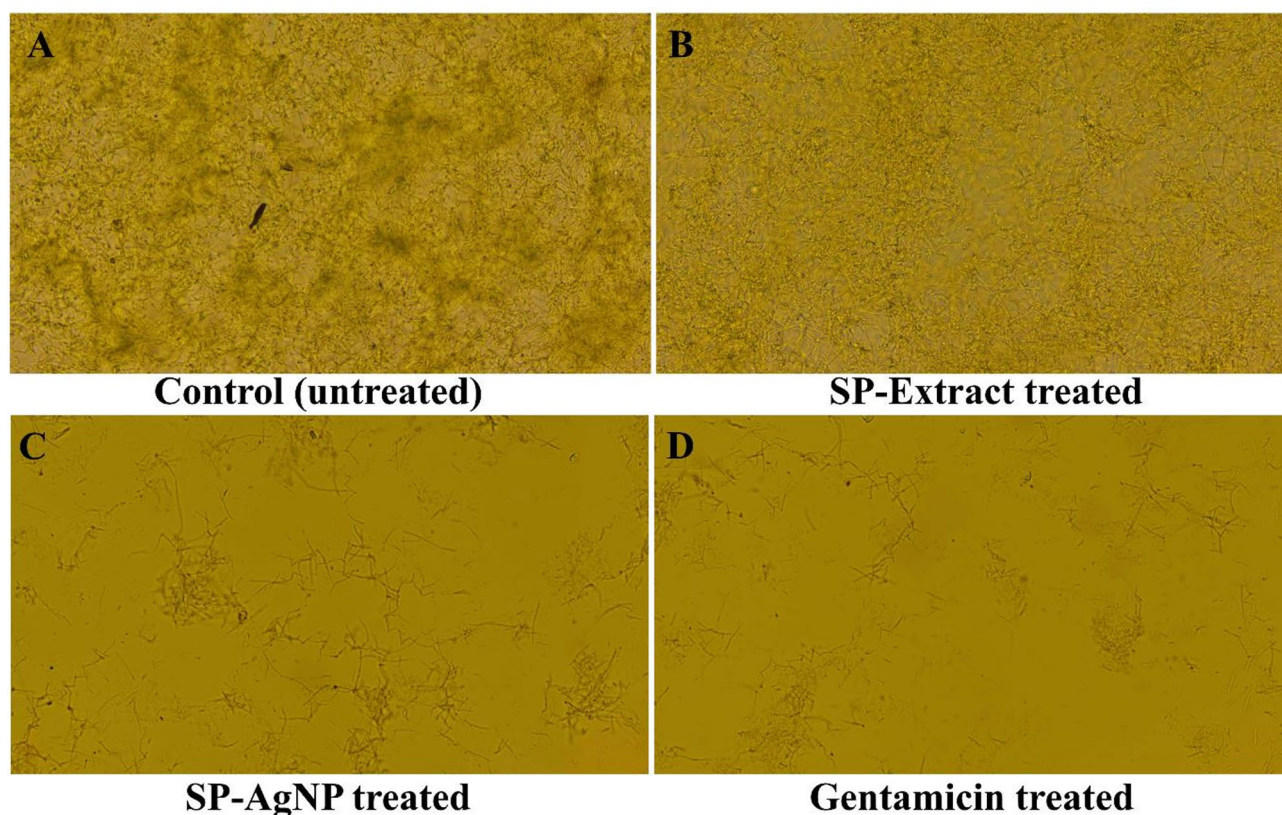
Fig. 8. (**A**) Effect of SP-AgNP on biofilm formation of *E. coli* at different doses with respect to untreated control (**B**). Motility of *E. coli* (i) in presence of SP-AgNPs at 175 μg/mL (ii) Control (untreated).

with crystalline characteristics (Fig. 3C). The FESEM micrographs additionally showed mild nanoparticle aggregation, likely due to the drying process during sample preparation. Despite this, the particles exhibited a relatively narrow size distribution and homogeneous surface morphology, further confirming the effective synthesis and stabilization of SP-AgNPs.

"Selected Area Electron Diffraction" referred to as SAED study of nanoparticles is a technique used in transmission electron microscopy (TEM) to analyze the crystal structure and orientation of individual nanoparticles. It works by focusing an electron beam on a specific small area of the sample generating a diffraction pattern that reveals information about the nanoparticle's lattice parameters and crystallinity. This study essentially allows researchers to determine the crystal structure of very small particles within a sample by examining the diffraction pattern produced when electrons interact with the crystal lattice of nano sized particles. In this study, the SAED image pattern indicated the face-centered cubic (fcc) lattice arrangement of SP-AgNPs (Fig. 4B).

Powder X-ray diffraction (XRD) is a non-destructive analytical technique employed to determine the crystal structure and identify the phases present in powdered materials. By examining the diffraction pattern generated when X-rays interact with the sample, XRD provides insights into the material's composition, degree of crystallinity, and lattice parameters. In the present study, XRD analysis of SP-AgNPs exhibited distinct diffraction peaks at 2θ angles of 38.07°, 44.16°, 64.39°, and 77.26°, corresponding to the (111), (200), (220), and (311) crystallographic planes, respectively (Fig. 4A). These peaks closely match the standard reference data from the ICDD PDF2 database (No. 071-4613), confirming the formation of face-centered cubic (fcc) structured silver nanoparticles. Morphological and elemental composition of the synthesized nanoparticles were evaluated by Transmission Electron Microscopy (TEM) coupled with Energy-Dispersive X-ray Spectroscopy (EDX) analysis.TEM-EDX is a widely used analytical tool for characterizing nanomaterials at high spatial resolution. In the present study, EDX spectra of SP-AgNPs exhibited a strong signal at 3 keV, which is a signature peak for elemental silver, confirming the complete reduction of Ag^+ ions to metallic Ag^0 (Fig. 3D). EDX profile of SP-AgNPs revealed the presence of
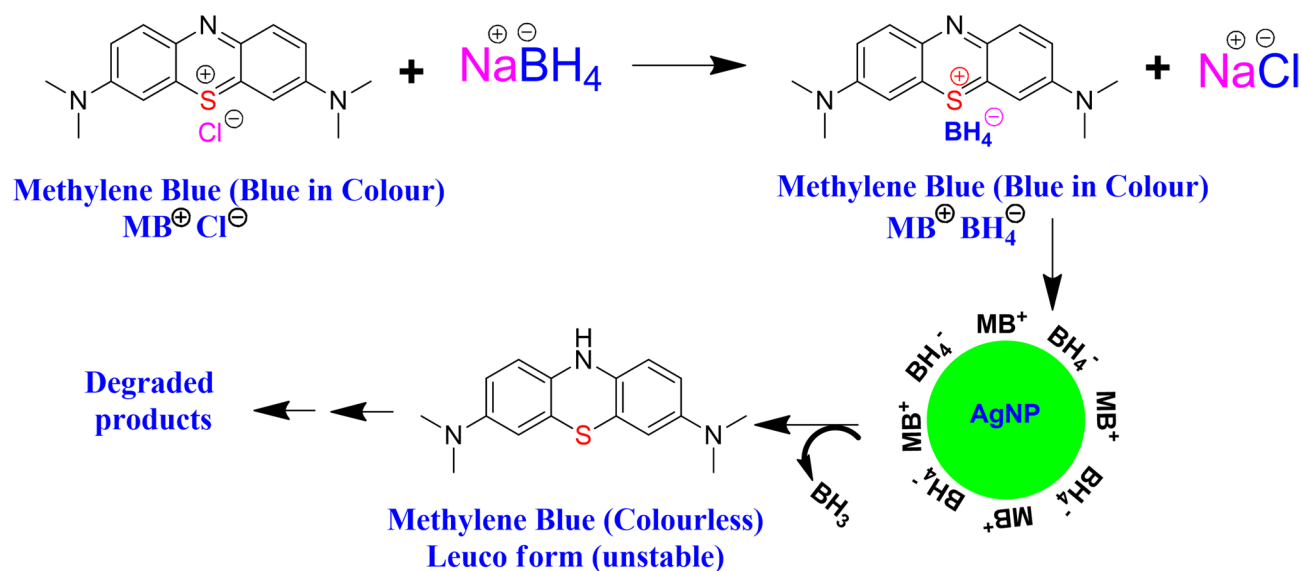
Fig. 9. Fluorescent microscopic images of biofilm inhibition studies with *E. coli*. (**A**) Biofilm formation of *E. coli* in control (untreated), (**B**) In presence of SP-Extract (**C**) In presence of SP-AgNPs and (**D**) In presence of gentamicin as standard.

carbon, oxygen, and chlorine and may be attributed to the presence of phytochemicals of *S. pinnata* bark extract as capping agents onto it. These findings collectively validate the successful biosynthesis of SP-AgNPs with fcc-arrangements of nanoparticles associated organic biomolecules on it's surface.

Additionally, X-ray Photoelectron Spectroscopy (XPS) was performed on the surface of SP-AgNPs to gain vital insights into their elemental composition and the oxidation states of silver. This analysis is crucial for understanding the nanoparticles' physicochemical characteristics and assessing their potential applications. In the present study, XPS analysis of SP-AgNPs (Fig. 5) revealed distinct peaks corresponding to C 1 s, O 1 s, and Ag 3 d, confirming the presence of these elements on the nanoparticle surface. The high-resolution spectrum of silver (Ag 3 d) (Fig. 5C) exhibited two prominent peaks at 368.2 eV and 374.4 eV, corresponding to the Ag $3d^{5/2}$ and Ag $3d^{3/2}$ orbitals, respectively[47,49]. The binding energy separation (ΔE) of 6.2 eV between these two peaks is consistent with the characteristic value for metallic silver (Ag^0), confirming the complete reduction of Ag^+ ions to their elemental form[3,47,49]. Moreover, the absence of peaks corresponding to other metals in the wide scan survey spectrum confirms the chemical purity of the synthesized silver nanoparticles.

Catalytic dye degradation potential of SP-AgNPs

Among the diverse applications of silver nanoparticles (AgNPs), their catalytic role in environmental remediation, particularly in dye degradation, remains critically important[26–32]. Industrial effluents from textile processing often contain recalcitrant dyes such as methylene blue (MB), which pose ecological threats and require efficient decolorization strategies[31,32]. In this study, SP-AgNPs were evaluated for their ability to catalyze the $NaBH_4$ mediated degradation of MB. This study revealed that $NaBH_4$ alone or SP-AgNPs alone exhibited only moderate degradation activity ($R^2 = 0.88901$) (Fig. 6B, C) while the combination of $NaBH_4$ and SP-AgNPs (w/w 1:1) led to a maximum degradation efficiency of 86% (Fig. 6D). This enhancement is attributed to the formation of an electron relay system, where electrons are shuttled from BH_4^- (donor) to MB^+ (acceptor) via the AgNPs surface. Mechanistically, the negatively charged surface of SP-AgNPs (zeta potential: -37 mV) facilitates the adsorption of cationic MB^+ and anionic BH_4^-. According to the SHAB principle[60], Na^+ ions preferentially bind to Cl^-, leaving MB^+ to associate with BH_4^- on the SP-AgNP surface. This spatial arrangement enhances the nucleophilic hydride attack at the electrophilic centers of MB, reducing it to its leuco form, which subsequently undergoes decomposition (Fig. 10). The absence of such electron relay networking in individual treatments explains their limited efficacy.This notable enhancement in dye degradation underscores the potential of SP-AgNPs as eco-friendly nanocatalysts for industrial wastewater treatment, combining high efficiency with green synthesis advantages.

Fig. 10. Proposed mechanism for the MB dye degradation by NaBH$_4$ in presence of catalytic SP-AgNPs.

Antibiofilm and antimotility activity of SP-AgNPs

SP-AgNPs demonstrated significant antibiofilm activity against *E. coli*, as evidenced by reduced biofilm mass and altered morphology. This effect is likely mediated through the inhibition of quorum sensing (QS) pathways and EPS synthesis, which are essential for biofilm initiation and maturation. In planktonic bacteria, QS regulates intercellular communication, nutrient exchange, and surface colonization. In our study, treatment with SP-AgNPs at 175 µg/mL significantly disrupted bacterial aggregation and colonization mechanisms. Motility assays further revealed strong suppression of flagella-mediated movement in treated cells (Fig. 8B), indicating interference with bacterial sensing and attachment machinery such as pili, fimbriae, and flagella. This impairment of motility, likely due to SP-AgNPs induced perturbation of intracellular signaling cascades, compromises the bacteria's ability to organize into structured biofilms[39,40].

In a nut shell, SP-AgNPs likely inhibit biofilm formation through a multi-targeted approach, involving oxidative stress induction, membrane damage, interference with quorum sensing, and inhibition of motility and EPS production. These combined effects explain the substantial reduction in biofilm mass, motility, and bacterial aggregation observed in our study.

Conclusion

Under an optimized set of conditions *S. pinnata*-mediated silver nanoparticles (SP-AgNPs) were synthesized with dual-functional viz. antibacterial and catalytic potential. SP-AgNPs exhibited excellent catalytic activity in the degradation of MB dye, demonstrating their applicability in waste water treatment. In parallel, they showed significant antibacterial activities against *E. coli*, a standard biofilm-forming pathogen. The multifunctional efficacy of SP-AgNPs may be attributed to their size distribution, surface charge, and phytomolecule-based capping agents that have collectively involved to influence their physicochemical and biological interactions. These results underscore the promise of phytogenic SP-AgNPs as an environmentally benign potential nanomaterials. However, further investigations viz. detailed mechanistic studies, biocompatibilities are warranted before industrial-scale deployment and clinical translations.

Data availability

All data generated or analyzed during this study are included in this published article.

References

1. Joudeh, N. & Linke, D. Nanoparticle classification, physicochemical properties, characterization, and applications: a comprehensive review for biologists. *J. Nanobiotechnol.* **20** (1), 1–29 (2022).
2. Iravani, S., Korbekandi, H., Mirmohammadi, S. V. & Zolfaghari, B. Synthesis of silver nanoparticles: chemical, physical and biological methods. *Res. Pharm. Sci.* **9** (6), 385–406 (2014).
3. Kaliammal, R. et al. *Zephyranthes Candida* flower extract mediated green synthesis of silver nanoparticles for biological applications. *Adv. Powder Technol.* **32** (11), 4408–4419 (2021).
4. Chopra, H. et al. Green metallic nanoparticles: biosynthesis to applications. *Front. Bioeng. Biotechnol.* **10**, 1–29 (2022).
5. Bedlovičová, Z. Green synthesis of silver nanoparticles using actinomycetes. *Green Synthesis of Silver Nanomaterials*, 547–569 (2022). (2013).
6. Nayak, D., Pradhan, S., Ashe, S., Rauta, P. R. & Nayak, B. Biologically synthesised silver nanoparticles from three diverse family of plant extracts and their anticancer activity against epidermoid A431 carcinoma. *J. Colloid Interface Sci.* **457**, 329–338 (2015).

7. Shu, M. et al. Biosynthesis and antibacterial activity of silver nanoparticles using yeast extract as reducing and capping agents. *Nanoscale Res. Lett.* **15** (1), 1–9 (2020).

8. Krishnaraj, C. et al. Synthesis of silver nanoparticles using *Acalypha indica* leaf extracts and its antibacterial activity against water borne pathogens. *Colloids Surf. B:Biointerfaces.* **76**, 50–56 (2010).

9. Mustapha, T., Misni, N., Ithnin, N. R., Daskum, A. M. & Unyah, N. Z. A review on plants and microorganisms mediated synthesis of silver nanoparticles, role of plants metabolites and applications. *Int. J. Environ. Res. Public. Health.* **19** (2), 674–690 (2022).

10. Liaqat, N. & Jahan, N. Green synthesized silver nanoparticles: optimization, characterization, antimicrobial activity, and cytotoxicity study by hemolysis assay. *Front. Chem.* **10**, 1–13 (2022).

11. Velsankar, K. et al. Green inspired synthesis of ZnO nanoparticles and its characterizations with biofilm, antioxidant, anti-inflammatory, and anti-diabetic activities. *J. Mol. Struct.* **1255**, 132420 (2022).

12. Velsankar, K., Sudhahar, S., Parvathy, G. & Kaliammal, R. Effect of cytotoxicity and a antibacterial activity of biosynthesis of ZnO hexagonal shaped nanoparticles by *Echinochloa frumentacea* grains extract as a reducing agent. *Mater. Chem. Phys.* **239**, 121976 (2020).

13. Ołdak, E. & Trafny, A. Secretion of proteases by *Pseudomonas aeruginosa* biofilms exposed to secretion of proteases by *Pseudomonas aeruginosa* biofilms exposed to Ciprofloxacin. *Antimicrob. Agents Chemother.* **49** (8), 3281–3288 (2005).

14. Qurashi, A. W. & Sabri, A. N. Biofilm formation in moderately halophilic bacteria is influenced by varying salinity levels. *J. Basic. Microbiol.* **52** (5), 566–572 (2012).

15. Kumar, L., Chhibber, S. & Harjai, K. Zingerone inhibit biofilm formation and improve antibiofilm efficacy of Ciprofloxacin against *Pseudomonas aeruginosa* PAO1. *Fitoterapia* **90**, 73–78 (2013).

16. Hall-stoodley, L., Costerton, J. W. & Stoodley, P. Bacterial biofilms: from the natural environment to infectious diseases. *Nat. Rev. Microbiol.* **2** (2), 95–108 (2004).

17. Bosso, J. A.The antimicrobial armamentarium: Evaluating current and future treatment options. *Pharmacotherapy*,25(10 II), 55S-62S (2005).

18. Yakandawala, N., Gawande, P. V., LoVetri, K. & Madhyastha, S. Effect of ovotransferrin, Protamine sulfate and EDTA combination on biofilm formation by catheter-associated bacteria. *J. Appl. Microbiol.* **102** (3), 722–727 (2007).

19. Wagner, V. E. & Iglewski, B. H. *P. aeruginosa* biofilms in CF infection. *Clin. Rev. Allergy Immunol.* **35** (3), 124–134 (2008).

20. Sharma, S. et al. Microbial Biofilm: A Review on Formation, Infection, Antibiotic Resistance, Control Measures, and Innovative Treatment.*Microorganisms*,11(6), 1614 (2023).

21. Swidan, N. S., Hashem, Y. A., Elkhatib, W. F. & Yassien, M. A. Antibiofilm activity of green synthesized silver nanoparticles against biofilm associated enterococcal urinary pathogens. *Sci. Rep.* **12** (1), 3869 (2022).

22. Ansari, M. A., Khan, H. M., Khan, A. A., Cameotra, S. S. & Pal, R. Antibiofilm efficacy of silver nanoparticles against biofilm of extended spectrum β-lactamase isolates of *Escherichia coli* and *Klebsiella pneumoniae*. *Appl. Nanosci.* **4** (7), 859–868 (2014).

23. Shafreen, R. B., Seema, S., Ahamed, A. P., Thajuddin, N. & Ali Alharbi, S. Inhibitory effect of biosynthesized silver nanoparticles from extract of *Nitzschia palea* against curli-mediated biofilm of *Escherichia coli*. *Appl. Biochem. Biotechnol.* **183** (4), 1351–1361 (2017).

24. Hosnedlova, B. et al. Effect of biosynthesized silver nanoparticles on bacterial biofilm changes in *S. aureus* and *E. coli*. *Nanomaterials* **12** (13), 2183 (2022).

25. Velsankar, K. et al. Bio-derived synthesis of MgO nanoparticles and their anticancer and hemolytic bioactivities. *Biocatal. Agric. Biotechnol.* **53**, 102870 (2023).

26. Shanker, U., Rani, M. & Jassal, V. Degradation of hazardous organic dyes in water by nanomaterials. *Environ. Chem. Lett.* **15** (4), 623–642 (2017).

27. Palani, G. et al. Silver nanoparticles for waste water management. *Molecules* **28** (8), 3520 (2023).

28. Gola, D. et al. Silver nanoparticles for enhanced dye degradation. *Curr. Res. Green. Sustain. Chem.* **4**, 100132 (2021).

29. Bharathi, D. et al. Kiwi fruit Peel Biowaste mediated green synthesis of silver nanoparticles for enhanced dye degradation and antibacterial activity. *Waste Biomass Valor.* **15** (3), 1859–1868 (2024).

30. Githala, C. K., Raj, S., Dhaka, A., Mali, S. C. & Trivedi, R. Phyto-fabrication of silver nanoparticles and their catalytic dye degradation and antifungal efficacy. *Front. Chem.* **10**, 1–17 (2022).

31. Oladoye, P. O., Ajiboye, T. O., Omotola, E. O. & Oyewola, O. J. Methylene blue dye: toxicity and potential elimination technology from wastewater. *Results Eng.* **16**, 100678 (2022).

32. Ogundare, S. A. et al. Catalytic degradation of methylene blue dye and antibacterial activity of biosynthesized silver nanoparticles using *Peltophorum pterocarpum* (DC.) leaves. *Environ. Sci. : Adv.* **2** (2), 247–256 (2022).

33. Laksemi, D. A. & A. Biological activity of *Spondias pinnata*: A review. *Indones J. Biomed. Sci.* **13** (2), 88–93 (2019).

34. Sameh, S., Al-Sayed, E., Labib, R. M. & Singab, A. N. Genus Spondias: A Phytochemical and Pharmacological Review. *Evid. Based Complement. Alternat. Med.*, 1–13 (2018). (2018).

35. Ghate, N. B., Hazra, B., Sarkar, R. & Mandal, N. In vitro anticancer activity of *Spondias pinnata* bark on human lung and breast carcinoma. *Cytotechnology* **66**, 209–218 (2014).

36. Hazra, B., Biswas, S. & Mandal, N. Antioxidant and free radical scavenging activity of *Spondias pinnata*. *BMC Complement. Altern. Med.* **8**, 1–10 (2008).

37. Li, R. et al. Chemical composition and the cytotoxic, antimicrobial, and anti-inflammatory activities of the fruit Peel essential oil from *Spondias pinnata* (anacardiaceae) in xishuangbanna, Southwest China. *Molecules* **25** (2), 1–13 (2020).

38. Manik, M. K. & Islam, S. M. Investigation of in vitro antioxidant, antimicrobial and thrombolytic activity of the exocarp of *Spondias pinnata* (Anacardiaceae). *Can. Chem. Trans.* **1** (3), 191–201 (2013).

39. Das, M. C. et al. Vitexin alters *Staphylococcus aureus* surface hydrophobicity to obstruct biofilm formation. *Microbiol. Res.* **263**, 127126–127140 (2022).

40. Das, M. C., Sandhu, P., Gupta, P., Rudrapaul, P., De, U. C., Tribedi, P., … Bhattacharjee,S. Attenuation of Pseudomonas aeruginosa biofilm formation by Vitexin: A combinatorial study with azithromycin and gentamicin.Sci. Rep., 6, 1–13(2016).

41. Salvioni, L. et al. Negatively charged silver nanoparticles with potent antibacterial activity and reduced toxicity for pharmaceutical preparations. *Int. J. Nanomed.* **12**, 2517–2530 (2017).

42. Vinayagam, R. et al. Structural characterization of marine macroalgae derived silver nanoparticles and their colorimetric sensing of hydrogen peroxide. *Mater. Chem. Phys.* **313**, 128787 (2024).

43. Goudarzi, M., Mir, N., Mousavi-Kamazani, M., Bagheri, S. & Salavati-Niasari, M. Biosynthesis and characterization of silver nanoparticles prepared from two novel natural precursors by facile thermal decomposition methods. *Sci. Rep.* **6**, 1–13 (2016).

44. Velsankar, K., Preethi, R., Ram, P. S. J., Ramesh, M. & Sudhahar, S. Evaluations of biosynthesized ag nanoparticles via *Allium sativum* flower extract in biological applications. *Appl. Nanosci.* **10** (9), 3675–3691 (2020).

45. Velsankar, K., Parvathy, G., Sankaranarayanan, K., Mohandoss, S. & Sudhahar, S. Green synthesis of silver oxide nanoparticles using *Panicum miliaceum* grains extract for biological applications. *Adv. Powder Technol.* **33** (7), 103645 (2022).

46. Cecere, D., Bruno, A., Minutolo, P. & D'Alessio, A. DLS measurements on nanoparticles produced in laminar premixed flames. *Synth. Met.* **139** (3), 653–656 (2003).

47. Motas, J. G., Gorji, N. E., Nedelcu, D., Brabazon, D. & Quadrini, F. XPS, SEM, DSC and nanoindentation characterization of silver Nanoparticle-Coated biopolymer pellets. *Appl. Sci.* **11** (16), 7706 (2021).

48. Ali, M. H. et al. Analysis of crystallographic structures and properties of silver nanoparticles synthesized using PKL extract and nanoscale characterization techniques. *ACS Omega.* **8** (31), 28133–28142 (2023).

49. Al-Gaashani, R., Zakaria, Y., Gladich, I., Kochkodan, V. & Lawler, J. XPS, structural and antimicrobial studies of novel functionalized Halloysite nanotubes. *Sci. Rep.* **12** (1), 21633 (2022).
50. Joseph, S. & Mathew, B. Facile synthesis of silver nanoparticles and their application in dye degradation. *Mater. Sci. Eng. B.* **195**, 90–97 (2015).
51. Vijayaram, S. et al. Applications of green synthesized metal Nanoparticles - a review. *Biol. Trace Elem. Res.* **202** (1), 360–386 (2024).
52. Anandan, S., Ponnusamy, K., Ashokkumar, M. & V., & A review on hybrid techniques for the degradation of organic pollutants in aqueous environment. *Ultrason. Sonochem.* **67**, 105130 (2020).
53. Magureanu, M., Mandache, N. B. & Parvulescu, V. I. Degradation of organic dyes in water by electrical discharges. *Plasma Chem. Plasma Process.* **27** (5), 589–598 (2007).
54. Suvith, V. S. & Philip, D. Catalytic degradation of methylene blue using biosynthesized gold and silver nanoparticles. *Spectrochim Acta Mol. Biomol. Spectrosc.* **118**, 526–532 (2014).
55. Vanaja, M. et al. Degradation of methylene blue using biologically synthesized silver nanoparticles. *Bioinorg. Chem. Appl.* **2014** (1), 742346 (2014).
56. Jain, A. et al. Multi dye degradation and antibacterial potential of Papaya leaf derived silver nanoparticles. *Environ. Nanotechnol Monit. Manag.* **14**, 100337 (2020).
57. Alamier, W. M. et al. Green synthesis of silver nanoparticles using *Acacia ehrenbergiana* plant cortex extract for efficient removal of Rhodamine B cationic dye from wastewater and the evaluation of antimicrobial activity. *ACS Omega.* **8** (21), 18901–18914 (2023).
58. Losasso, C. et al. Antibacterial activity of silver nanoparticles: sensitivity of different Salmonella serovars. *Front. Microbiol.* **5**, 1–9 (2014).
59. Kalwar, K. & Shan, D. Antimicrobial effect of silver nanoparticles (AgNPs) and their mechanism – a mini review. *Micro Nano Lett.* **13** (3), 277–280 (2018).
60. Pearson, R. G. Hard and soft acids and bases, HSAB, part 1: fundamental principles. *J. Chem. Educ.* **45** (9), 581 (1968).

Acknowledgements

Author contributions

U.C.D., M.C.D., and B.K.D. conceptualized and designed the study. B.K.D. conducted the synthesis, characterization and dye degradation activity study of SP-AgNPs. R.D. helps to perform the experiments to evaluate the dye degradation properties while M.C.D. performed experiments to assess the antibacterial and antibiofilm activity of SP-AgNPs. U.C.D., M.C.D., B.K.D., S.G., and A.G. contributed in writing and revision of the manuscript. All authors approved the final version of the manuscript.

Declarations

Competing interests

The authors declare no competing interests.

Additional information

Supplementary Information The online version contains supplementary material available at https://doi.org/10.1038/s41598-025-17558-1.

Correspondence and requests for materials should be addressed to U.C.D.

Reprints and permissions information is available at www.nature.com/reprints.

Publisher's note Springer Nature remains neutral with regard to jurisdictional claims in published maps and institutional affiliations.